Supporting Information

Magnetic and Thermodynamic Control of Coordination Network Crystallization using a Hexaazaphenalene-based Ligand

Qiao Jiang,[a] Hiroaki Suzuki,[a] Yuki Wada,[a] Xiaohan Wang,[b,c] Yoichi Murakami,[b,c] Takaya Matsumoto,[a,d] Pavel M. Usov[a] and Masaki Kawano[a*]

[a]Department of Chemistry, School of Science, Tokyo Institute of Technology; Meguro-ku, Tokyo 152-8550, Japan.

[b]Laboratory for Zero-Carbon Energy, Institute of Innovative Research, Tokyo Institute of Technology, Meguro-ku, Tokyo 152-8550, Japan

[c]Department of Mechanical Engineering, School of Engineering, Tokyo Institute of Technology, Meguro-ku, Tokyo 152-8552, Japan

[d]Central Technical Research Laboratory, ENEOS Corporation; Naka-ku, Yokohama, Kanagawa 231-0815, Japan

*Corresponding author. Email: mkawano@chem.titech.ac.jp

Content

Experimental

1. General information

All chemical reagents and solvents were purchased from commercial sources and used without further purification. ^{1}H (400 MHz) and ^{13}C NMR (100 MHz) spectra were measured using JEOL JNM-ECA400 II spectrometer. The sample was dissolved in deuterated dimethyl sulfoxide (DMSO-d_6), and the chemical shifts were referenced against the DMSO peak (δ = 2.5). Infrared (IR) spectra were measured on a Thermo Scientific Nicolet iS5 FT-IR spectrometer using the attenuated total reflectance (ATR) method. Elemental analysis was performed using J-Science Lab JM10 CHN Analyzer MICRO CORDER instrument. Powder X-ray diffraction (PXRD) patterns were collected on a Rigaku Miniflex powder diffractometer with D/teX Ultra (1D) detector using Cu Kα (λ = 1.54184 Å) radiation. The samples suspended in MeOH were placed onto a Si plate and covered with Mylar film to prevent solvent evaporation. Rigaku SmartLab diffractometer employing Ni-filtered Cu Kα (λ = 1.54184 Å) line focused radiation at 2000 W (40 kV, 50 mA) power was used for high resolution PXRD measurements. The sample suspended in MeOH was loaded into capillary tubes (borosilicate glass, inner diameter = 0.5 mm, outer diameter = 0.8 mm), which were flame sealed to prevent solvent evaporation. The patterns were collected using 1 ° min^{-1} scan speed and 120 rpm rotation rate for the capillary. Single crystal X-ray diffraction (SCXRD) data for Cd-4TPHAP-1 and Cd-4TPHAP-2 were collected at 123 K on a Rigaku Synergy-R/DWTI APEX II instrument with a Hypix-6000HE detector equipped with Rigaku GNNP low temperature device using PhotonJet-R X-ray source with MicroMax™-007 rotating anode Cu Kα radiation (λ = 1.54184 Å). The structures were solved by intrinsic phasing (SHELXT-2018) and refined by full-matrix least squares calculations on F^2 (SHELXL-2018) using the SHELX-TL program package. Crystal face indexes were obtained using CrysAlisPro 171.42.49 program based on the SCXRD data.

2. Synthetic methods

K(4-TPHAP):

The synthetic procedure was based on the previously published method,[1,2] with some modifications. Pyridine-4-carboximidamide hydrochloride (5.97 g, 38 mmol) and sodium tricyanomethanide (0.88 g, 7.8 mol) were ground together in a hot mortar which was pre-heated at 80 °C. about the solid mixture was transferred into a Teflon-lined stainless steel autoclave and heated at 200 °C for 20 h. After cooled down to room temperature, the crude mixture was dissolved in aqueous HCl solution (2 M). Acetone was added to the solution causing appearance of precipitate. It was collected by filtration, washed with acetone and dried. The crude compound was dissolved in H_2O and pH was adjusted to 10 using KOH solution (5 M). about theThe resultant suspension was stirred at 50 °C. After cooling down, the solid was isolated by filtration and washed with an ice-cold 1:2 MeOH/Ethyl acetate mixture. Finally, it was dried under vacuum at 50 °C to give the desired product as a dark yellow powder (2.17 g, 4.9 mmol, 63%). ^{1}H NMR (DMSO-d_6, 400 MHz) δ 8.77 (d, 6H), 8.40 (d, 6H). ^{13}C NMR (DMSO-d_6, 100 MHz) δ 104.8, 123.3, 147.3, 151.2, 167.0, 167.8. Elemental analysis calcd (%) for $C_{22}H_{23.4}N_9O_{5.7}K$ = $K(C_{22}H_{12}N_9)(H_2O)_{5.7}$: C, 48.56; H, 4.33; N, 23.06. Found: C, 48.55; H, 4.03; N, 23.06.

Crystallization of coordination networks (no magnetic field):

The synthesis was performed using a layer diffusion method. In 5 mL glass vials, three separate MeOH solutions were carefully layered on top of each other to avoid quick mixing: K(4-TPHAP) (1 mL, 1.4 mM, bottom layer), pure MeOH (1 mL, middle layer), and $Cd(ClO_4)_2 \cdot 6H_2O$ (1 mL, 4 mM, upper layer). The vials were placed in incubators at 3, 15 or 35 °C and a relative humidity of less than 30% for 4 days. Then, the solutions were decanted and the resultant yellow transparent crystals were washed with fresh MeOH and kept in MeOH.

Crystallization of coordination networks (with magnetic field):

Neodymium (NdFeB) disk magnets (diameter = 11 mm, thickness = 3.5 mm, B_{max} = 320 mT, measured using digital Tesla meter Model AMST-5) were placed into 5 mL glass vials. Three separate MeOH solutions were then carefully layered on top of each other to avoid quick mixing: K(4-TPHAP) (1 mL, 1.4 mM, bottom layer), pure MeOH (1 mL, middle layer), and $Cd(ClO_4)_2 \cdot 6H_2O$ (1 mL, 4 mM, upper layer). The vials were placed in incubators at 3, 15 or 35 °C and a relative humidity of less than 30% for 4 days. Then, the solutions were decanted and the resultant yellow transparent crystals were washed with fresh MeOH and kept in MeOH.

Cd-4TPHAP-1:

Pure crystalline powders and single crystals of Cd-4TPHAP-1 were obtained using 15 °C, 0 mT synthetic conditions. For elemental analysis and IR spectroscopy, the powders were filtered, washed with fresh MeOH and dried. Elemental analysis calcd (%) for $C_{22.62}H_{28.32}N_{9.09}O_{11.7}ClCd_2$ = $Cd_2(C_{22}H_{12}N_9)_{1.01}(ClO_4)(H_2O)_{7.3}(CH_3OH)_{0.4}$: C, 31.05; H, 3.26; N, 14.55; Cl, 4.05. Found: C, 30.71; H, 2.94; N, 14.18; Cl, 3.72.

Cd-4TPHAP-2:

Pure crystalline powders and single crystals of Cd-4TPHAP-2 were obtained using 3 °C, 320 mT synthetic conditions. For elemental analysis and IR spectroscopy, the powders were filtered, washed with fresh MeOH and dried. Elemental analysis calcd (%) for $C_{44}H_{49.4}N_{18}O_{13.74}Cl_{0.26}K_{0.26}Cd$ = $Cd(C_{22}H_{12}N_9)_2(H_2O)_{12.7}(KClO_4)_{0.26}$: C, 44.71; H, 4.21; N, 21.33. Found: C, 44.90; H, 4.09; N, 21.05.

Crystallization of coordination networks in thin cells:

To exclude the effects of the neodymium magnet surface on the network formation, the reactions were carried out inside thin cells (1 mm). Three separate solutions of MeOH were carefully layered to avoid quick mixing: K(4-TPHAP) (0.15 mL, 1.4 mM, bottom layer), pure MeOH (0.15 mL, middle layer), and $Cd(ClO_4)_2 \cdot 6H_2O$ (0.15 mL, 4 mM, upper layer). To apply a magnetic field, the thin cell was sandwiched between

two disk magnets. The network crystallization was performed at 15 °C, with and without magnetic field. The obtained crystals were visually inspected and photographed using an optical microscope (Leica M205 C microscope and Infinity Capture software) (Figure S3).

Transformation of Cd-4TPHAP-2 into Cd-4TPHAP-1:

Triangular crystals of Cd-4TPHAP-2 were synthesized using the 3 °C, 320 mT reaction and kept in the mother solution. The disk magnets were removed, and the reaction vials were placed in incubators at 3 or 35 °C for 5 days (Scheme S1). After that, the reaction solution was decanted and the resultant crystalline solid was washed with fresh MeOH. The powder patterns were collected in MeOH (Figure S6).

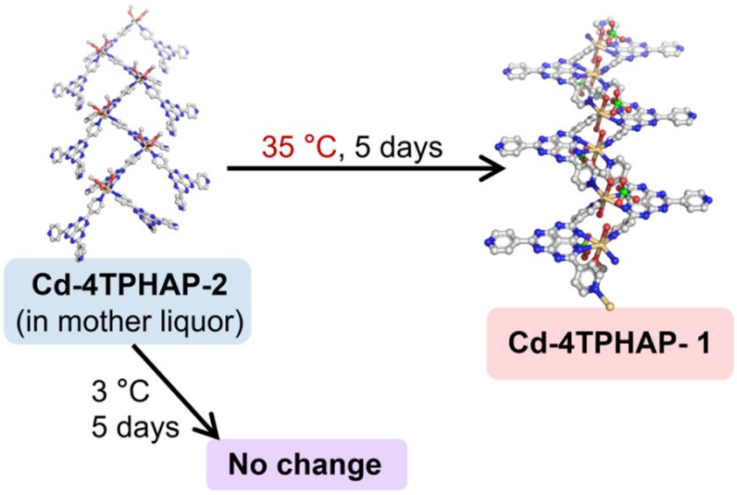

Scheme S1. The transformation of Cd-4TPHAP-2 into Cd-4TPHAP-1.

3. Calculation methods

Network transformation energy:

The changes of internal energy (ΔU) and Helmholtz free energy (ΔF) for the transformation of Cd-4TPHAP-2 into Cd-4TPHAP-1 (Figure S8a) were calculated using Matlantis. The calculations accommodating solvent effects were conducted by incorporating the solvent into a cell with periodic boundaries to match the liquid density (Figure S7a), which was created using the Python script named "liquid generator". Subsequently, all structural optimization and vibration calculations were executed using the standard script. Calculation mode was "CRYSTAL PLUS D3" and the PFP (PreFerred Potential) version was v5.0.0.[3,4] Additionally, there were no significant fluctuations in ΔU values between 3 and 35 °C (Figure S8b).

Magnetic susceptibility calculations using density functional theory (DFT):

Magnetic susceptibilities χ^{mol} (in cgs-ppm) for 4-TPHAP$^-$ in gas phase and K(4-TPHAP) in methanol were calculated using Gaussian 16 package[5] with Gauge-Independent Atomic Orbital (GIAO) method using PBE0 functional and 6-31G basis set.[6] Solvent effects from methanol were approximated by a polarizable continuum model (PCM).

Results

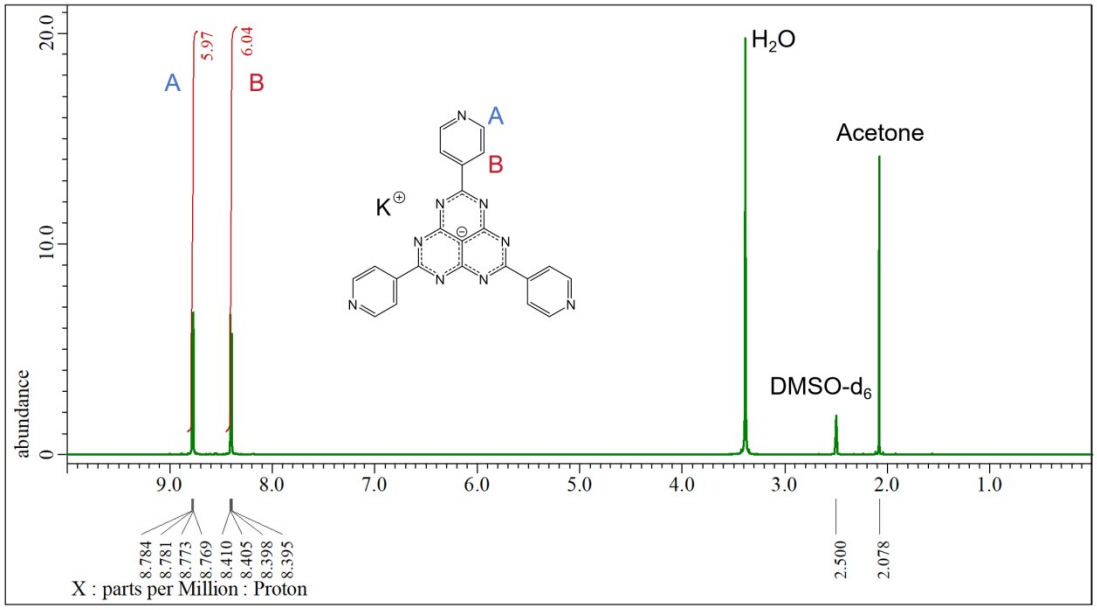

Figure S1. ^{1}H NMR (DMSO-d_6, 400 MHz) spectrum of K(4-TPHAP).

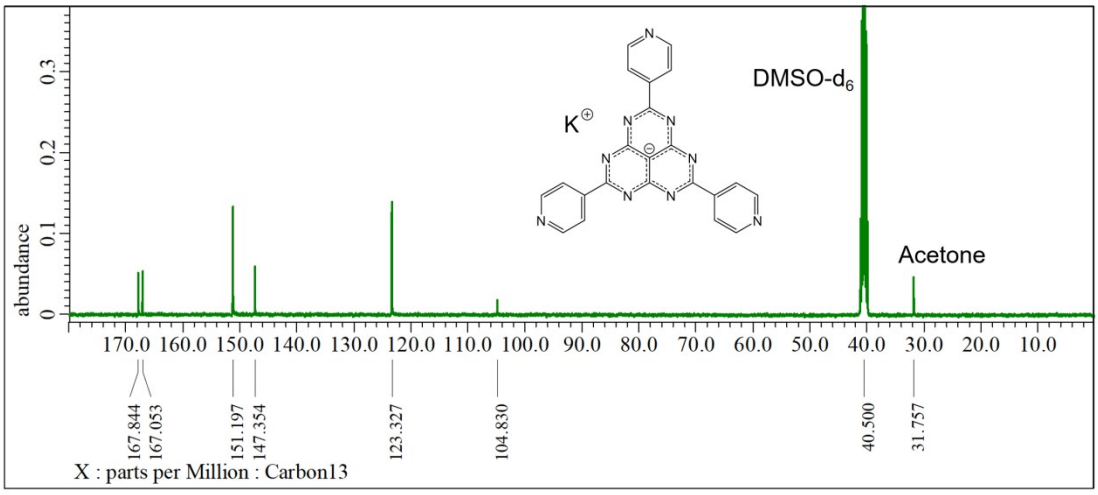

Figure S2. ^{13}C NMR (DMSO-d_6, 100 MHz) spectrum of K(4-TPHAP).

Table S1. Crystallographic data of Cd-4TPHAP-1 and Cd-4TPHAP-2.

Identification code	Cd-4TPHAP-1	Cd-4TPHAP-2
Empirical formula	$C_{53}Cd_2Cl_2N_{18}O_{24}H_{36}$	$C_{49.22}H_{31.48}CdN_{18}O_{16.89}$
Formula weight	1604.70	1268.45
Temperature/K	123.15	123.15
Crystal system	triclinic	orthorhombic
Space group	*P*-1	$Pca2_1$
a/Å	11.8103(1)	30.3621(3)
b/Å	12.5965(2)	7.96360(1)
c/Å	13.3862(2)	28.1930(2)
α/°	80.395(1)	90
β/°	84.225(1)	90
γ/°	78.443(1)	90
Volume/Å^3	1919.06(5)	6816.83(1)
Z	1	4
ρ_{calc} g/cm^3	1.389	1.226
μ /mm^{-1}	5.767	3.180
F(000)	802.0	2544.0
Crystal size/mm^3	0.15 × 0.13 × 0.075	0.205 × 0.175 × 0.095
Radiation	Cu Kα (λ = 1.54184)	Cu Kα (λ = 1.54184)
2Θ range for data collection/°	9.11 to 152.242	11.072 to 152.204
Reflections collected	35291	36119
Independent reflections	7898 [R_{int} = 0.0534, R_{sigma} = 0.0438]	10872 [R_{int} = 0.0388, R_{sigma} = 0.0313]
Data/restraints/parameters	7898/9/565	10872/22/980
Goodness-of-fit on F^2	1.055	1.036
Final R indexes [I>=2σ (I)]	R_1 = 0.0522, wR_2 = 0.1464	R_1 = 0.0540, wR_2 = 0.1510
Final R indexes [all data]	R_1 = 0.0557, wR_2 = 0.1500	R_1 = 0.0608, wR_2 = 0.1593
Completeness	0.999 (>135.4°)	0.998 (>135.4°)
CCDC deposit number	2339307	2339308

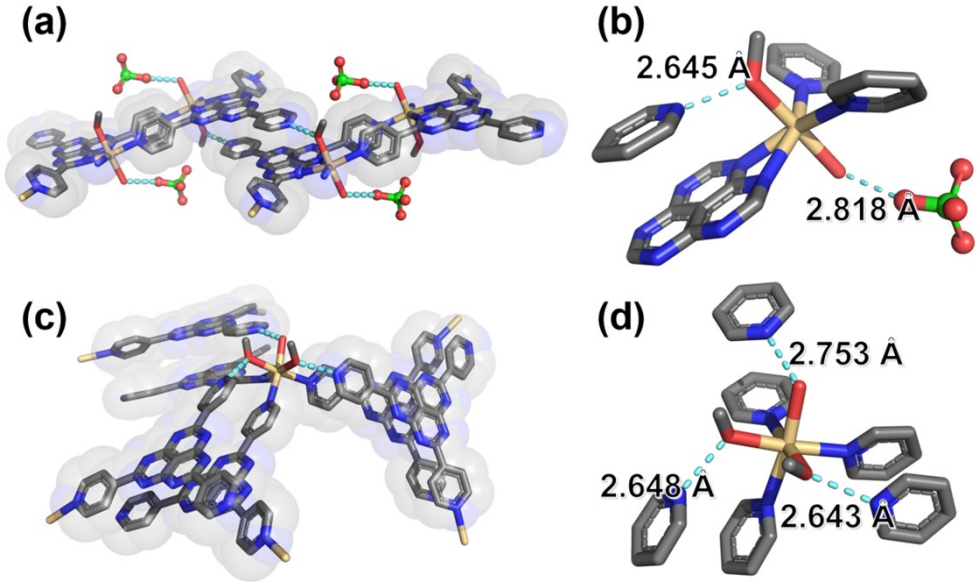

Figure S3. The interactions between the chains of Cd-4TPHAP-1 (a) Two kinds of hydrogen bonds around the Cd^{2+} center in Cd-4TPHAP-1 (b). The neighboring chains in Cd-4TPHAP-2 interacting through hydrogen bonding and π-π stacking (c). Three kinds of hydrogen bonds around the Cd^{2+} center in Cd-TPHAP-2 (d).

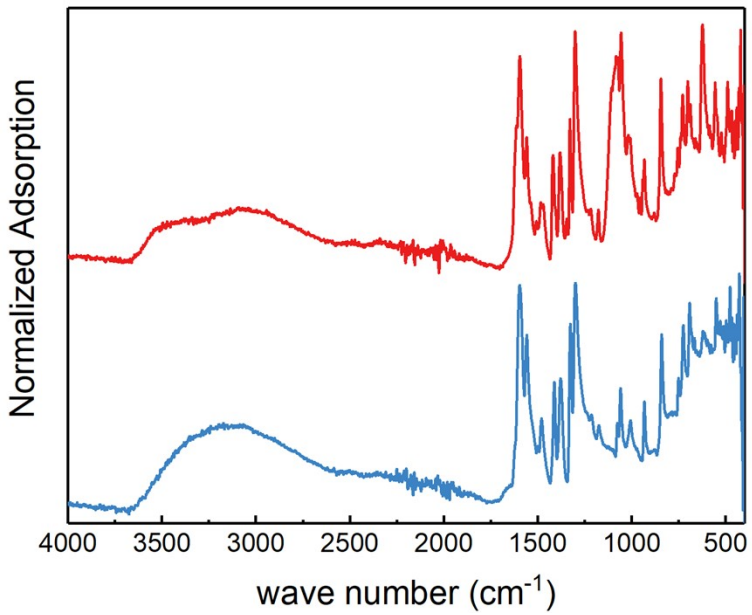

Figure S4. FT-IR spectra of Cd-4TPHAP-1 (*red*) and Cd-4TPHAP-2 (*blue*).

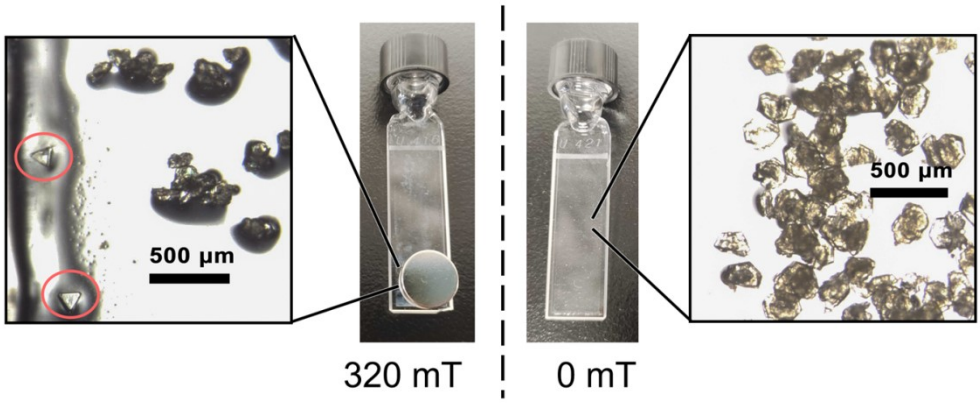

Figure S5. The photographs of thin cells after the network reaction with (*left*) and without (*right*) application of a magnetic field. Zoomed in sections show the obtained crystals. Red circles highlight the triangular prisms corresponding to Cd-4TPHAP-2.

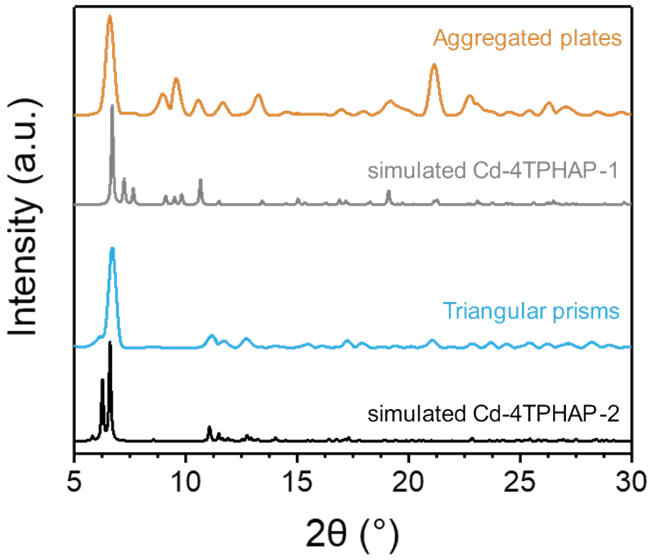

Figure S6. Powder patterns of aggregated plate and triangular prism crystals isolated from the thin cell measured using Rigaku Synergy-S and compared to the simulated patterns of Cd-4TPHAP-1 and Cd-4TPHAP-2.

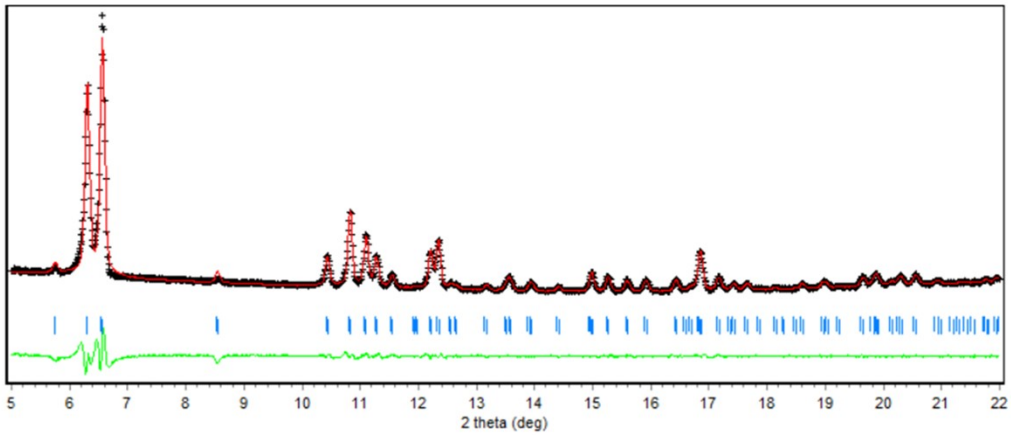

Figure S7. Le Bail refinement of the powder pattern of Cd-4TPHAP-2 measured in MeOH using a rotating capillary sample holder. Measured pattern (*black crosses*), Le Bail fit (*red solid line*), residual (*green solid line*) and allowed reflections for the $Pca2_1$ space group at Cu $K\alpha_1$ and $K\alpha_2$ radiation wavelengths (*blue tick marks*). The refinement was performed using Rietica.

Table S2. Unit cell parameters of Cd-4TPHAP-2 extracted from PXRD data using Le Bail refinement compared to the SCXRD data.

Unit cell ($Pca2_1$)	SCXRD (123 K)	PXRD (298 K)
a (Å)	30.3621(3)	30.63(8)
b (Å)	7.96360(10)	8.462(5)
c (Å)	28.1930(2)	27.96(7)
V (Å^3)	6816.8	7247.0

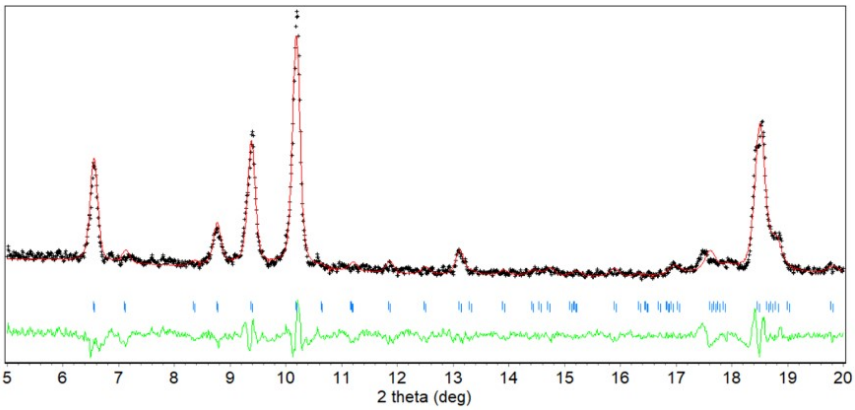

Figure S8. Le Bail refinement of the powder pattern of Cd-4TPHAP-1 obtained at 35 °C and 0 mT measured in MeOH using a Si plate sample holder. Measured pattern (*black crosses*), Le Bail fit (*red solid line*), residual (*green solid line*) and allowed reflections for the *P-1* space group at Cu $K\alpha_1$ and $K\alpha_2$ radiation wavelengths (*blue tick marks*). Fitted unit cell parameters: a = 10.80(4) Å, b = 12.8(1) Å, c = 13.4(1) Å, α = 80(3)°, β = 92(2)° and γ = 75(2)°.

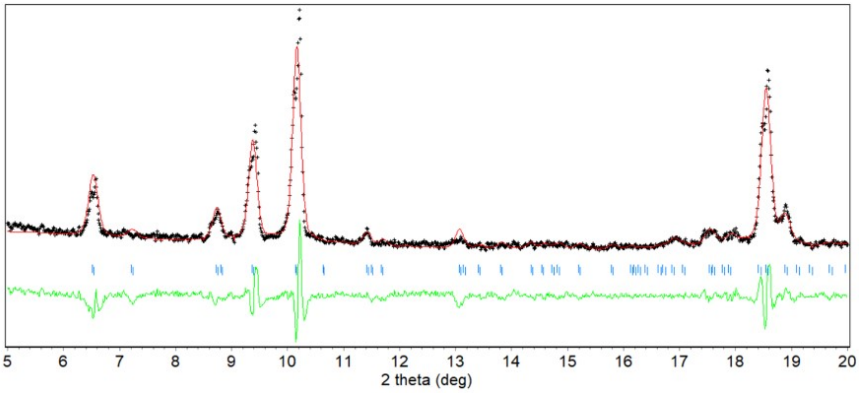

Figure S9. Le Bail refinement of the powder pattern of Cd-4TPHAP-1 obtained at 35 °C and 320 mT measured in MeOH using a Si plate sample holder. Measured pattern (*black crosses*), Le Bail fit (*red solid line*), residual (*green solid line*) and allowed reflections for the *P-1* space group at Cu $K\alpha_1$ and $K\alpha_2$ radiation wavelengths (*blue tick marks*). Fitted unit cell parameters: a = 10.65(6) Å, b = 12.9(1) Å, c = 13.7(1) Å, α = 81(4)°, β = 95(3)° and γ = 72(2)°.

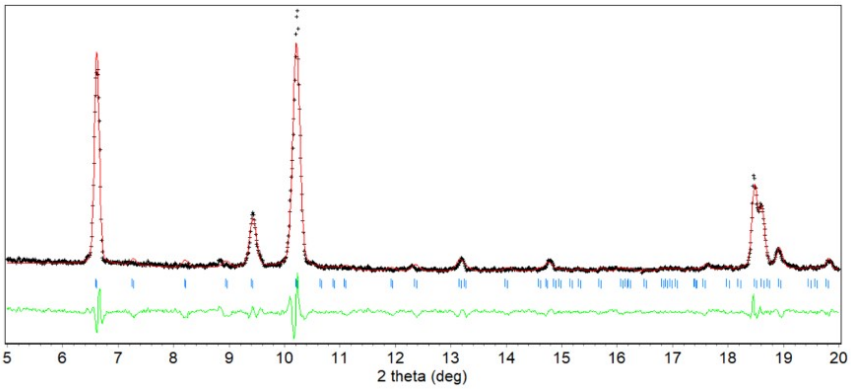

Figure S10. Le Bail refinement of the powder pattern of Cd-4TPHAP-1 obtained at 15 °C and 0 mT measured in MeOH using a Si plate sample holder. Measured pattern (*black crosses*), Le Bail fit (*red solid line*), residual (*green solid line*) and allowed reflections for the *P-1* space group at Cu $K\alpha_1$ and $K\alpha_2$ radiation wavelengths (*blue tick marks*). Fitted unit cell parameters: a = 11.12(4) Å, b = 12.72(5) Å, c = 13.51(8) Å, α = 82(2)°, β = 91(2)° and γ = 74.9(7)°.

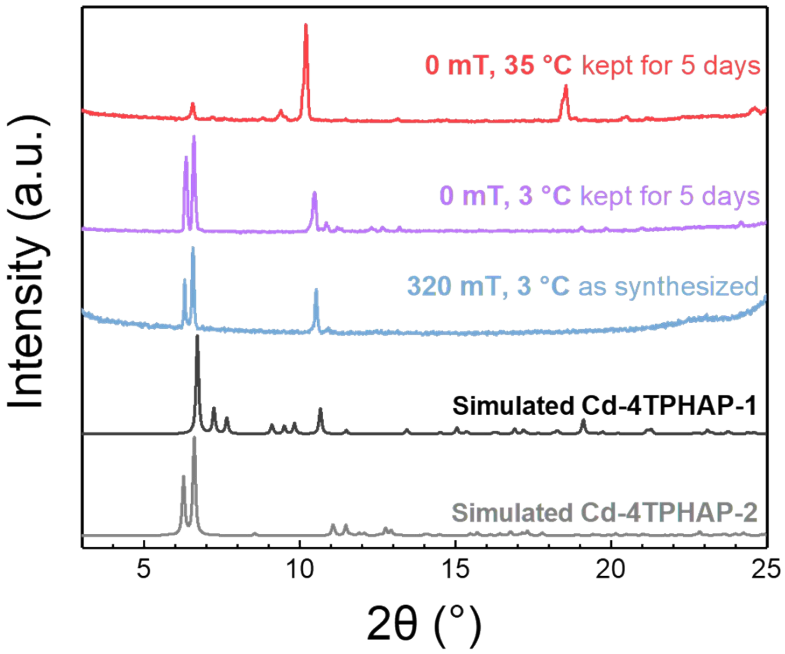

Figure S11. Powder patterns of the as synthesized Cd-4TPHAP-2 (*blue*) and the products of transformation reactions performed at 3 (*purple*) and 35 °C (*red*). The predicted patterns of Cd-4TPHAP-1 and Cd-4TPHAP-2 are shown for reference.

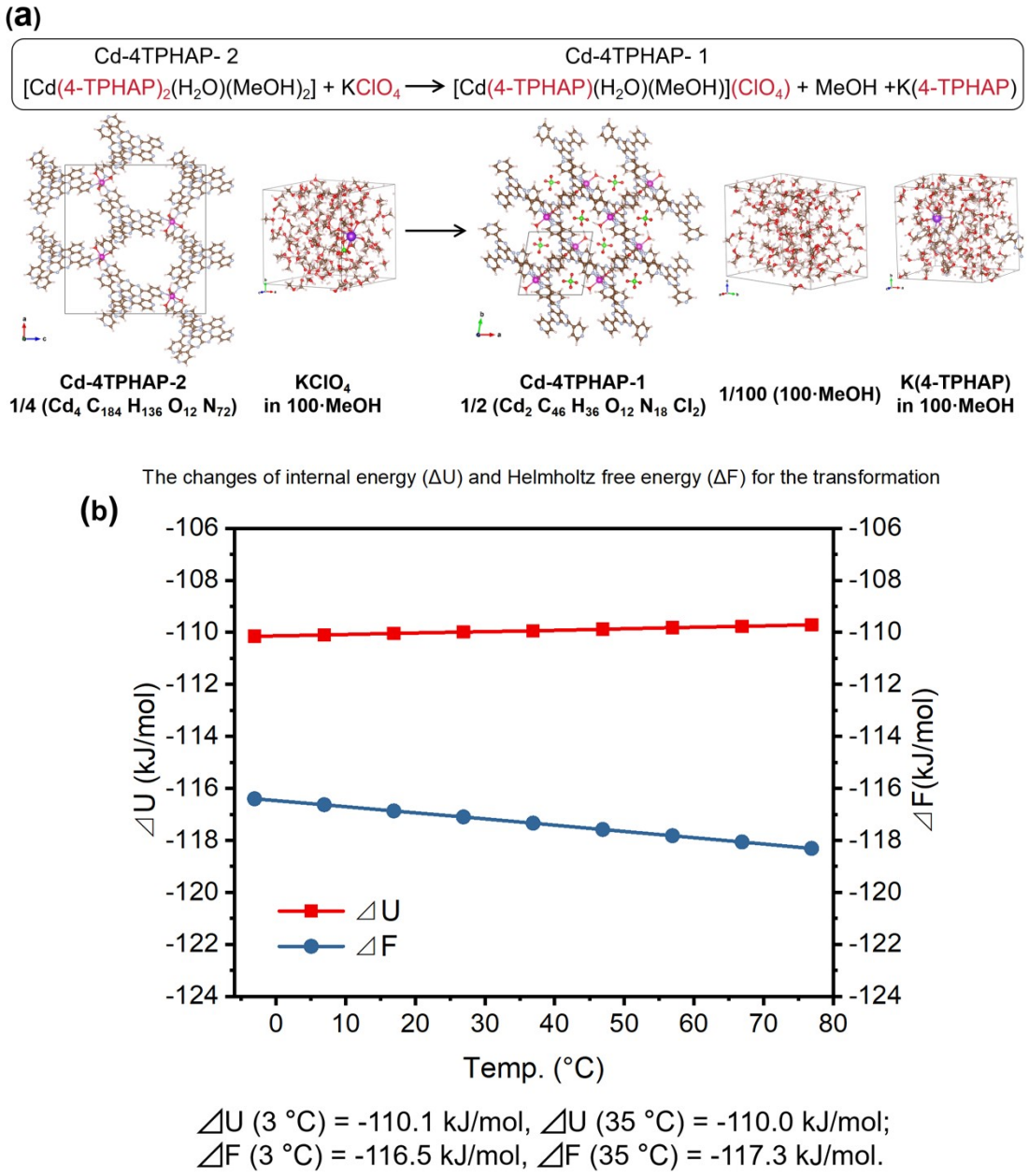

Figure S12. a) The full reaction scheme for the transformation of Cd-4TPHAP-2 into Cd-4TPHAP-1 and the calculation model of cells with periodic boundaries. b) The changes in ΔU and ΔF with temperature.

Table S3. Calculated anisotropic magnetic susceptibility values for 4-TPHAP$^-$ in gas phase and K(4-TPHAP) in MeOH. where χ_{min}, χ_{mid} and χ_{max} are three eigenvalues obtained after diagonalization, $\chi_{iso} = 1/3(\chi_{min} + \chi_{mid} + \chi_{max})$ is the isotropic average and $\Delta\chi_{an} = \chi_{max} - \chi_{min}$ is the anisotropy. The energy between the maximum and minimum susceptibility directions (ΔE) was calculated using equation 1 where B = 320 mT.

Specie	Calculated χ^{mol} (in cgs-ppm)					ΔE (kJ/mol)
	χ_{min}	χ_{mid}	χ_{max}	χ_{iso}	$\Delta\chi_{an}$	
4-TPHAP$^-$ (Gas phase)	-120.88	-120.88	-409.67	-217.15	-288.79	0.296
K(4-TPHAP) (in MeOH)	-140.57	-147.52	-410.00	-232.69	-269.43	0.276

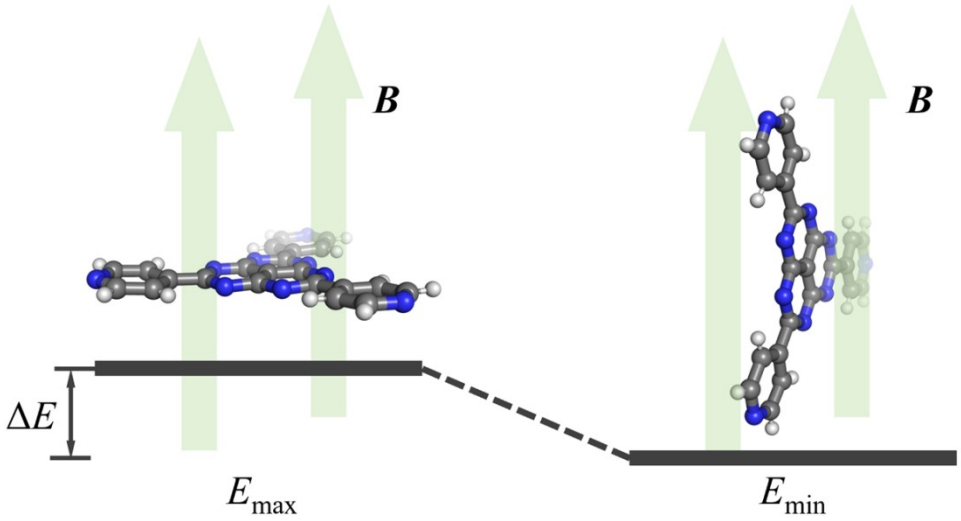

Figure S13. The two orientations of 4-TPHAP$^-$ relative to the applied magnetic field (***B***): perpendicular and parallel. The associated energies are shown as E_{max} and E_{min} in the magnetic field, respectively, and the energy difference between the two states is represented by ΔE.

References

1 Y. Yakiyama, A. Ueda, Y. Morita, M. Kawano, *Chem. Commun.*, 2012, **48**, 10651–10653.

2 K. Nakanishi, H. Ohtsu, G. Fukuhara, M. Kawano, *Chem. Eur. J.*, 2019, **25**, 15182–15188.

3 S. Takamoto, C. Shinagawa, D. Motoki, K. Nakago, W.-W. Li, I. Kurata, T. Watanabe, Y. Yayama, H. Iriguchi, Y. Asano, T. Onodera, T. Ishii, T. Kudo, H. Ono, R. Sawada, R. Ishitani, M. Ong, T. Yamaguchi, T. Kataoka, A. Hayashi, N. Charoenphakdee, T. Ibuka, *Nat. Commun.*, 2022, **13**, 2991.

4 Matlantis (https://matlantis.com/), software as a service style material discovery tool.

5 M. J. Frisch, G. W. Trucks, H. B. Schlegel, G. E. Scuseria, M. A. Robb, J. R. Cheeseman, G. Scalmani, V. Barone, G. A. Petersson, H. Nakatsuji, X. Li, M. Caricato, A. V. Marenich, J. Bloino, B. G. Janesko, R. Gomperts, B. Mennucci, H. P. Hratchian, J. V. Ortiz, A. F. Izmaylov, J. L. Sonnenberg, F. Williams, F. Ding, F. Lipparini, J. Egidi, B. Goings, A. Peng, T. Petrone, D. Henderson, V. G. Ranasinghe, J. Zakrzewski, N. Gao, G. Rega, W. Zheng, M. Liang, M. Hada, K. Ehara, R. Toyota, J. Fukuda, M. Hasegawa, T. Ishida, Y. Nakajima, O. Honda, H. Kitao, T. Nakai, K. Vreven, J. A. Throssell, A. Montgomery Jr., J. E. Peralta, F. Ogliaro, M. J. Bearpark, J. J. Heyd, E. N. Brothers, K. N. Kudin, V. N. Staroverov, T. A. Keith, R. Kobayashi, J. Normand, K. Raghavachari, A. P. Rendell, J. C. Burant, S. S. Iyengar, J. Tomasi, M. Cossi, J. M. Millam, M. Klene, C. Adamo, R. Cammi, J. W. Ochterski, R. L. Martin, K. Morokuma, O. Farkas, J. B. Foresman, D. J. Fox, *Gaussian 16*, revision C.01; Gaussian, Inc.: Wallingford, CT, 2016.

6 R. Guo, M. N. Uddin, L. S. Price, S. L. Price, *J. Phys. Chem. A.*, 2020, **124**, 1409–1420.